Pressure measurements in a stretched vortex

Frédéric Moisy[1] and Philippe Petitjeans[2]

[1] Laboratoire de Physique Statistique, ENS, 24 rue Lhomond, 75231 Paris Cedex 05 (France)
[2] Laboratoire de Physique et Mécanique des Milieux Hétérogènes, ESPCI, 10 rue Vauquelin, 75231 Paris (France)

Abstract. We report new results obtained with a strong laboratory vortex, generated between rotating disks with an axial stretching, providing a model of strong vortex structures present in turbulent flows. We first characterize the strength of the vortex in this geometry by means of a global pressure measurement, and give direct evidence of a mechanism of stretching saturation due to strong rotation. Pressure measurements are then performed with a miniature probe sensor close to the vortex, in order to study the relevance of bulk measurements with small but invasive sensors. We analyze the influence of some geometric characteristics of the probe (size, distance from the vortex) on the measured pressure, together with the influence of the presence of a probe on the vortex strength. We briefly discuss consequences of these observations on pressure measurements in the bulk of turbulent flows.

1 Introduction

Vorticity filaments are known to play a central role in turbulent flows [1], and particularly in the intermittency of energy dissipation. Experimentally, it is tempting to investigate these filaments through their core depression [2]. This pressure is related to the characteristics of the vortex such as vorticity, diameter, and stretching. However, because of the invasive character of conventional pressure probes, very little is known about the pressure fluctuations in the bulk of turbulent flows. Most of the time, measurements are performed on the wall [3–5], and are not easily related to the bulk properties. Let us mention here recent progress in non invasive quantitative measurements, with acoustic [6–8] and cavitation [9,10] techniques.

In this paper, we first describe a non intrusive method to measure the mean pressure of an isolated stretched vortex generated between rotating disks. Then, classical local measurements with a pressure probe are analyzed and compared with the other technique described here.

2 Experimental set-up

The experiment is performed in a large water tank, and the flow is driven between two smooth disks, 10 cm in diameter, rotating in the same sense (see figure 1). The frequency can be adjusted from 0 to 25 Hz. In the center of each disk, a 0.5 cm diameter hole is made which is used to create an axial pumping. The

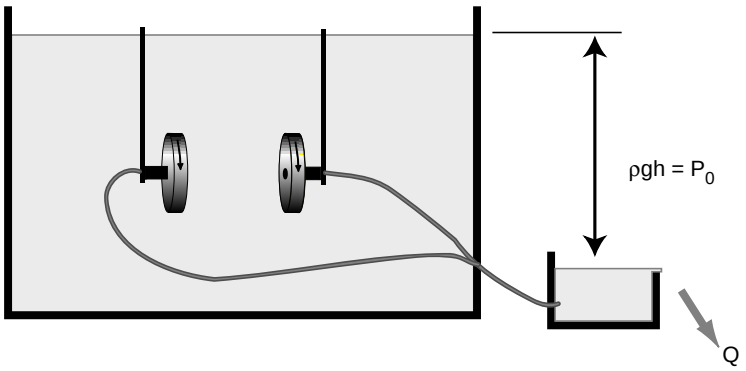

Fig. 1. Experimental set-up.

suction is generated by gravity, from a constant level auxiliary tank, under the main tank level. The imposed level difference h, between 0 and 90 cm, allows to impose a depression $P_0 = \rho g h$ between 0 and 90 mbar.

The axial velocity from the center to a hole due to the suction ranges from 0 to 5 m/s, leading to a mean axial velocity gradient $\langle \gamma_z \rangle \simeq \langle \partial U_z / \partial z \rangle$ from 0 to 50 s^{-1}. The combined effects of rotation and stretching generate a strong vortex (see figure 2), slowly precessing in the same direction as its rotation. The stability of this vortex has been extensively studied by Manneville *et al.* [7], by means of an ultrasound scattering technique [8].

The water leaving the auxiliary tank allows an accurate measurement of the flow rate Q (within 1 %). This flow rate is related to the mean axial stretching,

$$\langle \gamma_z \rangle = \frac{Q}{4Sd},$$

where S is the hole area and d the distance between the disks. The measured flow rate lies between 0 and 3 L/min, and depends both on the imposed suction pressure and on the frequency of the disks. In the absence of rotation of the disks, the imposed depression P_0 leads to a flow rate Q_0. Varying the height of the auxiliary tank we perform a calibration $Q_0 = F(P_0)$. Inverting this calibration allows to deduce, from the measurement of Q, the actual pressure P in the presence of the vortex.

The control parameters are (Ω, P_0, d), where $\Omega = 2\pi f$ is the disk frequency. In the experiments described in this paper the distance d has been kept fixed to 10 cm, and only (Ω, P_0) are varied.

3 Global measurement and vortex characterization

In the absence of disk rotation, a suction pressure P_0 is imposed and a constant flow rate Q_0 is measured. When the disks begin to rotate, after a few seconds, the flow rate decreases from Q_0 to a smaller value Q. From this change we can

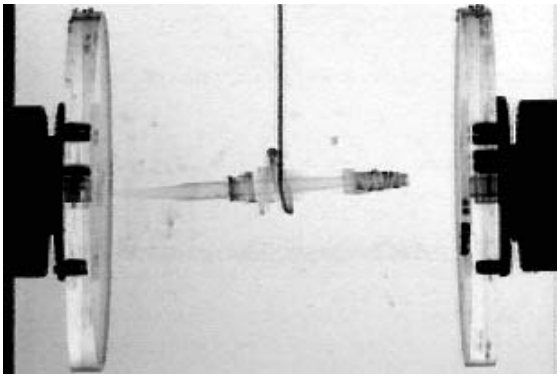

Fig. 2. Visualization of the stretched vortex. Dye is injected in the periphery of the vortex, through the vertical tube in the center.

deduce the pressure change at the axis level, inverting the calibration $Q = F(P)$ described above. The new pressure at the axis is then given by

$$P'_{\text{axis}} = P_{\text{axis}} + P_0 - F^{-1}(Q),$$

We then define $\Delta P = |P'_{\text{axis}} - P_{\text{axis}}|$ as the magnitude of this depression, which can be seen as the depression caused by the presence of the stretched vortex. We will hereafter note ΔP the vortex depression; we have ΔP=0 in the absence of disk rotation [$Q = Q_0 = F(P_0)$]. Since this procedure is based on a calibration covering the whole range of pressure and flow rate, it is free of assumption and gives confidence in the determination of the vortex depression.

Figure 3 shows measurements of the vortex depression ΔP for increasing disks velocity, at two different suction depressions P_0. We can see, for each case, two different regimes: the first one, called the "linear regime", for low disks velocity, corresponds to vortex depressions roughly behaving as $\Delta P \propto f$. After some frequency limit, depending on the suction depression, a new behavior arises, called the "saturated regime", where the vortex depression remains constant as the frequency is increased. This vortex depression ΔP is found to be slightly lower than the suction depression P_0.

The vortex depressions, normalized by the suction depressions, are found to collapse well, when plotted versus the non dimensional ratio

$$B = \left(\frac{\rho \Omega^2 R^2}{P_0}\right)^{1/2}, \tag{1}$$

where R is the disk radius. $\rho\Omega^2 R^2$ can be interpreted as the depression caused by a solid-body rotation due to the disk rotation, in the absence of axial pumping. However, the R dependence of B has to be checked in more detail, performing new experiments with different disk diameters. Figure 4 shows measurements of the normalized vortex depressions versus B, for 8 different suction depressions

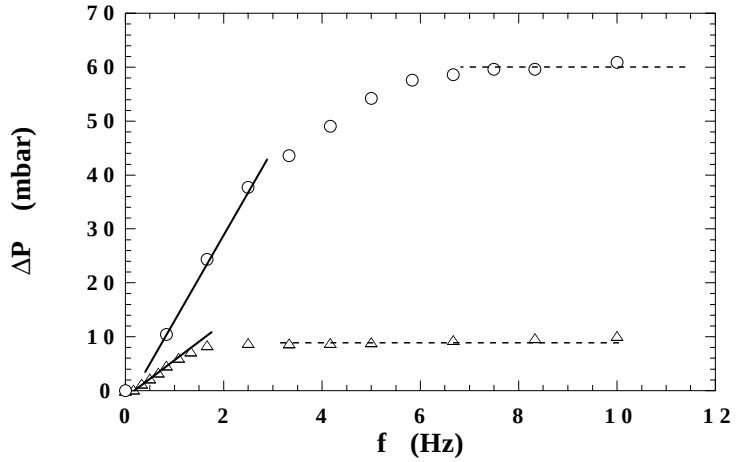

Fig. 3. Vortex depression ΔP versus disk frequency f, for two different suction pressures. $\triangle$: $P_0 = 10$ mbar and $\circ$: $P_0 = 70$ mbar. Solid lines indicate the linear regimes and dashed lines the saturated regimes.

P_0, ranging from 20 to 90 mbar. These curves are well fitted by the empirical formula

$$\frac{\Delta P}{P_0} = \sigma \tanh\left(\frac{B - B_s}{B_c}\right), \tag{2}$$

where B_s represents the lower threshold, below which there is no measurable vortex depression, and B_c represents the cross-over between the linear and the saturated regimes. For large values of B, the normalized depression saturates to the limiting value σ. We obtain $B_s \simeq 0.02$ and $B_c \simeq 0.38$, with no noticeable dependence on P_0. Values of σ are found to lie around 0.85 ± 0.05. We observe a very slow increase of σ for increasing P_0, but this effect seems to be very weak (less than 10 % for the range of P_0 we have spanned) and may allow to consider σ as a constant. The fact that $\sigma < 1$ means that the vortex never becomes strong enough to invert the flow rate, *i.e.* to pump the auxiliary tank water through the holes.

The saturation of $\Delta P/P_0$ for $B > B_c$ can be understood in terms of rotation–stretching interaction. For low frequencies ($B < B_c$), the axial suction is very efficient and highly enhances the low vorticity level injected by the disks. In this regime the vortex becomes relatively strong. For higher values of the frequency, the vorticity becomes important and tends to bidimensionalize the flow, reducing the axial strain. The stretching becomes less efficient, and unable to enhance vorticity any more. The vortex pressure tends to saturate at some ratio of the suction depression, given by $\sigma \simeq 0.85$. This saturating value may result from the equilibrium between the enhancement of rotation by stretching and the decrease of stretching by rotation.

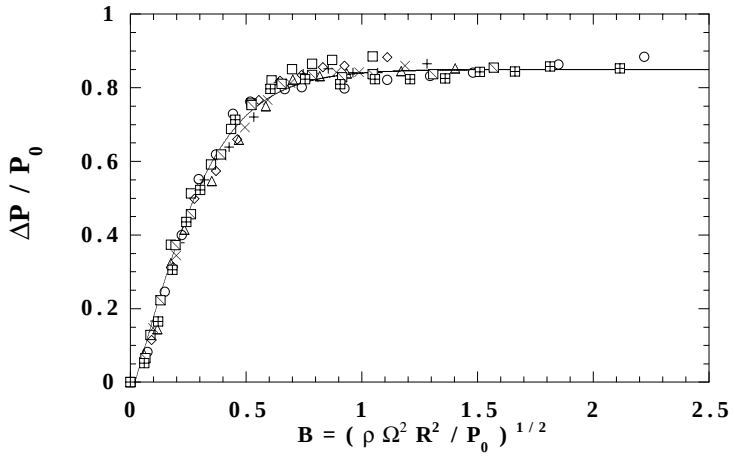

Fig. 4. Normalized vortex depressions $\Delta P/P_0$ versus the rotation–stretching ratio B. The different symbols represent 8 different suction depressions P_0 from 20 to 90 mbar. The full line is a best fit by the empirical formula (2), with $B_s = 0.02$, $B_c = 0.38$ and $\sigma = 0.85$.

The $\Delta P \propto \Omega$ behavior of the linear regime allows to deduce some scaling properties of this vortex. Manneville *et al* [7] have shown that in this regime the circulation Γ behaves as $\Omega^{3/4}$. Writing the depression as $\Delta P \sim \rho u_{\theta\max}^2$, where $u_{\theta\max}$ is the maximum azimuthal velocity, and the circulation as $\Gamma \sim u_{\theta\max} r_c$ (r_c is the vortex core radius), we can deduce

$$u_{\theta\max} \sim \Omega^{1/2}, \qquad r_c \sim \Omega^{1/4}.$$

Nothing is known about the vortex properties in the saturated regime. New experiments, using both acoustic and pressure measurements, are needed to provide more insight into these behaviors, and to characterize in more details the transition between the two regimes.

When the frequency is increased to higher values ($B \simeq 5$), we observe a new behavior (not shown here): The normalized vortex pressure begins to decrease from the saturated value σ down to much lower values (around $\sigma/2$). This may be due to vortex instabilities occurring at this higher Reynolds numbers: The vortex becomes unstable, breaks up and another one is generated. The measured pressures then result from a time-averaged flow rate, and can be interpreted as a mean value of the pressure due to the break up and reforming vortex. Indeed, in order to confirm this scenario, dye visualizations are needed, but are hard to perform because of the high speeds involved. Another explanation may come from a change in the forcing efficiency, due to the thinning of the boundary layer at higher frequencies.

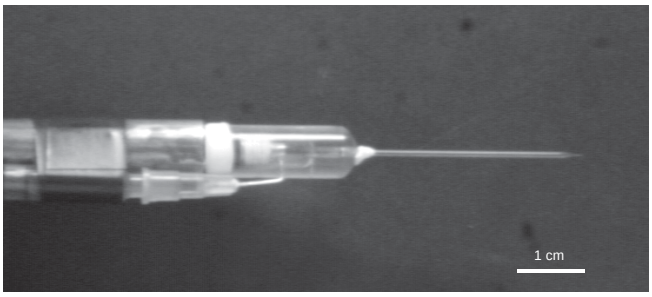

Fig. 5. The pressure probe consists of a piezoelectric transducer, placed at the end of a 200 µm diameter capillary tube. The needle, connected to a syringe, allows to expel residual air bubbles in the cavity, causing pressure fluctuation damping.

4 Pressure sensor and local measurements

We are now interested in more classical local measurement ot the pressure near the vortex core. Here, the aim is to characterize the measurement itself by an invasive detector, and additionally to estimate the vortex perturbation by the presence of the probe in this configuration.

The pressure measurements are performed using a piezoelectric transducer (see figure 5), 5 mm in diameter, placed in a water filled cavity, connected to a small glass tube. In order to minimize perturbations due to the presence of this probe in the flow, we make use of a fine capillary tube, whose initial diameter is 1 mm, which can be stretched down to 50 µm. We denote ϕ the tube external diameter (the internal diameter is around 0.7 ϕ). The viscous damping frequency is around 10^5 Hz, and the vortex shedding frequency around 1 kHz for the typical velocities involved here. The most limitating constraint is given by the resonnance frequency of the cavity, which is above 100 Hz for the smallest diameter. The pressure probe position is controlled by a 3D displacement system, with 1 µm accuracy. The distance from the probe to the disk axis is denoted r_s, and for the present experiments the probe is kept at mid-distance between the disks.

Because of the slow precession, the vortex frequently sweeps in the close vicinity of the pressure probe, causing a sharp pressure drop. Figure 6 shows a typical pressure time series, when the pressure sensor is at a distance r_s=1 mm from the axis. In this example, the probe diameter at the tube end is ϕ = 260 µm. The pressure drops can reach −80 mbar, a value rather low compared to the solid-body rotation pressure $\frac{1}{2}\rho U_{\rm disk}^2 \simeq 13$ mbar and to the mean dynamic pressure caused by the axial stretching, $\frac{1}{2}\rho U_z^2 \simeq 30$ mbar. The mean waiting time between successive events is 1.9 s, leading to a mean precession frequency $f_p \simeq 0.5$ Hz $\simeq f_{\rm disk}/10$, a value in good agreement with ultrasound scattering measurements [7].

Two distributions of the pressure fluctuations are plotted on Figure 7, for two different probe distances, $r_s = 1$ and 4 mm. Pressure drops caused by the vortex

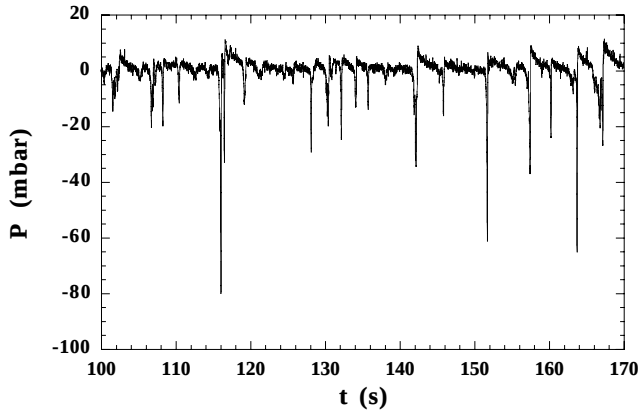

Fig. 6. Typical time series of pressure. The slight overshoot following the sharp drops are due to residual air microbubbles in the sensor cavity. $f_{\rm disk}$=5.1 Hz, $Q = 2 \times 3$ L/min, and $\phi = 260$ µm.

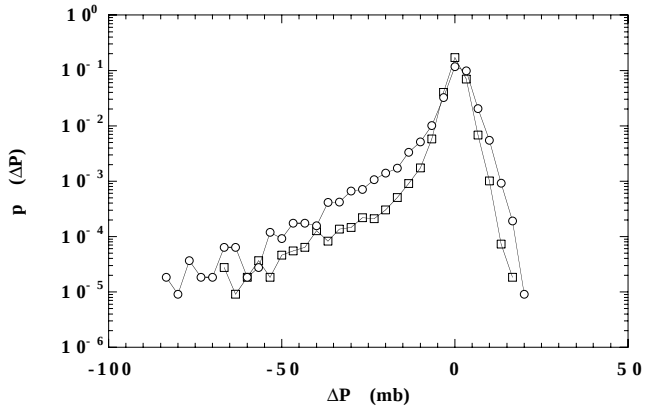

Fig. 7. Distribution of pressure for two distances, circle: $r_s = 1$ mm and square: $r_s = 4$ mm. $f_{\rm disk}$=5.1 Hz, $Q = 2 \times 3$ L/min, and $\phi = 260$ µm.

sweeping account for the large negative tails of these distributions, which can be roughly fitted by exponentials for $\Delta p < -15$ mbar. Their width, around 3 mbar, give a rough measure of the noise level. The slight positive tail is mainly due to an overshoot following the pressure drops, possibly caused by the presence of residual air microbubbles in the sensor cavity.

We can see that the further the probe is from the axis, the rarer the pressure drops. However, the slope of the negative tails remains unchanged for different values of r_s. This suggests that, for large r_s, the pressure drops typically reach the same values, but the vortex sweeps less frequently in the probe vicinity. As r_s is increased, the negative tail decreases and vanishes for $r_s \geq 8$ mm; this value

is found to be independent of the the disk frequency, and gives a rough estimate of the precession radius.

From the mean width Δt of the pressure drops, we can estimate the core size r_c of the vortex. For the measurements performed with the $\phi = 260$ µm sensor, we obtain $\Delta t = 160 \pm 60$ ms, leading to

$$r_c = \frac{2\pi R_p f_p}{\Delta t} \simeq 1 \ \text{mm}.$$

where $2\pi R_p f_p$ is the mean precession velocity, typically 5 mm/s, obtained from a mean precession radius $R_p \simeq 6$ mm and the precession frequency $f_p \simeq 0.5$ Hz. Although the uncertainty is high, this estimation of $r_c \simeq 1$ mm is in qualitative agreement with measurements of Manneville *et al.*[7]. It does not seem to depend on the probe diameter, at least for $\phi < 1$ mm.

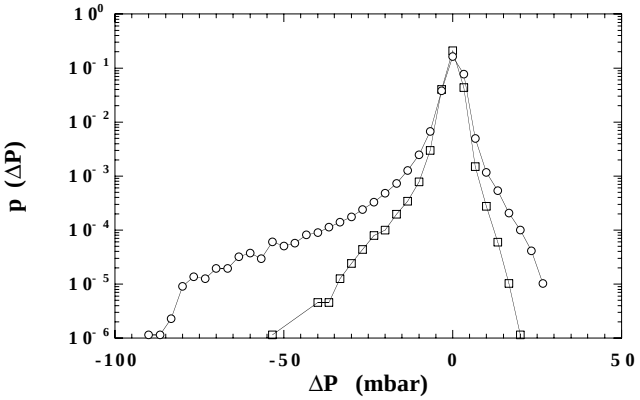

Fig. 8. Distribution of pressure for two probe sizes, at $r_s = 3$ mm. Circle: $\phi = 260$ µm, square: $\phi = 1$ mm. The best fit by an exponential $\exp[\Delta P/\alpha]$ for $\Delta p < -15$ mbar leads to $\alpha = 17$ mbar for $\phi = 260$ µm, and $\alpha = 6.7$ mbar for $\phi = 1$ mm.

We will now address the delicate issue of the influence of the probe on the vortex characteristics. Figure 8 shows two pressure distributions, at the same distance from the axis $r_s = 3$ mm, for two different probe sizes $\phi = 0.26$ mm and 1 mm. As in figure 7, the negative tails can be well fitted by exponentials, for $\Delta p < -15$ mbar. But, in contrast with figure 7, where the exponential slope is not affected by the distance r_s, now we can see that it is strongly decreased in the case of the bigger probe. This clearly indicates the strong influence of the probe size on the local pressure measurement.

It is important to determine whether this influence originates from the probe characteristics, or from a change in the vortex itself due to the presence of the probe; both are relevant in the context of pressure measurements in the bulk of turbulent flows. A detailed comparison between global measurements, described

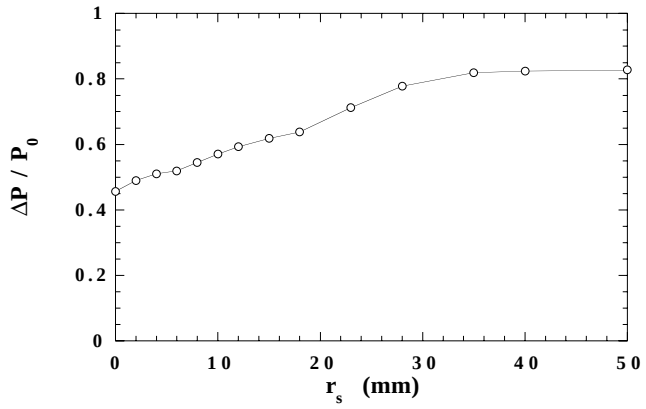

Fig. 9. Vortex depression ΔP normalized by the imposed suction depression P_0 in the saturated regime ($B = 1.05$), versus the probe distance from the axis r_s (diameter $\phi = 0.7$ mm).

in the previous section, and local measurements is in progress. Preliminary results are given on figure 9, which represents the change of the global vortex depression with the probe distance from the axis r_s. For $r_s > 40$ mm, we obtain $\Delta P/P_0 = \sigma \simeq 0.83$, in good agreement with the figure 4 in the saturated regime ($B = 1.05 \sim 3B_c$). When r_s is decreased down to 0, the rescaled depression falls down to $\Delta P/P_0 = 0.45$, meaning that the vortex (time-averaged) depression is roughly twice as small as withous the probe. Even when the probe is farther than the mean precession radius ($R_p \simeq 8$ mm), the vortex depression is strongly decreased.

Visualization by means of dye injected in the periphery of the vortex (as in figure 2) shows that no instability occurs when r_s is larger than a few probe diameter ϕ. These observations suggest that, even when the vortex remains stable, the presence of the probe at a distance $r_s < 10r_c$ significantly decreases its strength. This clearly illustrates the long-range sensitivity of such vortex to localized perturbation. Synchronized visualizations together with local pressure measurements are needed to get more insight into this behavior.

5 Discussion and Conclusion

In this paper we have reported first results obtained with a new experiment allowing to generate a strong and controlled stretched vortex. Two kinds of pressure measurements have been performed, global and local.

The global time-averaged pressure measurement allows to characterize the vortex strength for different rotation rates Ω and suction depressions P_0. We give evidence of a transitional behavior between two regimes, labeled with the non-dimensional ratio $B = (\rho\Omega^2 R^2/P_0)^{1/2}$, measuring the relative magnitude of the rotation effect compared to the stretching effect. For $B < B_c \simeq 0.38$,

stretching highly enhances the small level of vorticity injected by the disks, and the vortex depression is found to scale as B. For $B > B_c$, the strong rotation tends to saturate the stretching efficiency, which is unable to strengthen the vortex any more. In this second regime, the vortex depression ΔP saturates at the final value σP_0, where P_0 is the imposed suction depression and σ is found to be 0.85 ± 0.05. These observations are in good agreement with those of Nore *et al.* [11], who investigated both numerically and experimentally the rotation–stretching interaction mechanisms. The originality of our experimental set-up is to keep the flow rate Q (thus the stretching) free to adjust with the actual vorticity, giving clear evidence of the stretching saturation effect of the strongly rotating flow. We plan to use this global pressure measurement together with the ultrasound scattering technique [8,7] to investigate the circulation, vorticity and vortex radius evolution in these two regimes, and in particular to understand the observed values of the threshold B_c and the saturation ratio σ.

Local measurements, by means of conventional invasive probes, have been performed too, in order to investigate the relevance of bulk measurements in turbulent flows. In the particular configuration of a strong vortex in a quiet background flow, we show that such a method provides a reasonable measurement of the pressure drops, whose magnitude is in qualitative agreement with values obtained via the global measurements described above. However, we give evidence of a strong influence on both the probe size and the vortex–probe distance. These two effects are presumably due to the probe characteristics itself, and to the perturbation of the flow caused by the presence of the probe. This second point is illustrated by the strong decrease (by a factor 2) of the vortex depression in the presence of the probe, even when it remains farther than the mean precession radius.

These observations are of great importance in the context of pressure measurements in the bulk of turbulent flows. It appears that depressions caused by vortices whose radii are smaller than the probe size are likely to be missed, not only because of a spatial averaging effect, but essentially by perturbation of the flow caused by the probe itself. We mention here that the use velocity measurements by means of hot wire anemometry to detect small scale filaments [12], the mean advection velocity (typically one order of magnitude higher than the fluctuating velocity) makes the advection time lower than the typical timescale of perturbation. In this case, the measurement is believed not to be affected by the finite probe size. More work has to be done in order to clarify what is due to a pure probe size effect, and what is due to the perturbation of the vortex in this geometry.

The authors acknowledge G. Baque and F. Botausci for experimental helps, and S. Manneville, A. Maurel, V. Emsellem, P. Tabeling and H. Willaime for fruitful discussions.

References

1. U. Frisch: Turbulence, the legacy of A.N. Kolmogorov. Cambridge University Press, Cambridge (1995).

2. S. Douady, Y. Couder, and M.E. Brachet: Direct observation of the intermittency of intense vorticity filaments in turbulence *Phys. Rev. Lett.* **67** (8), 983–986 (1991).
3. O. Cadot, S. Douady and Y. Couder: Characterization of the low pressure filaments in a 3D turbulent shear flow *Phys. Fluids* **7**, 630 (1995).
4. P. Abry, S. Fauve, P. Flandrin, and C. Laroche : Analysis of pressure fluctuations in swirling turbulent flows *J. Phys. II France* **4** 725–733 (1994).
5. P. Chaisnais, P. Abry, and J.-F. Pinton: Intermittency and coherent structures in a swirling flow: a wavelet analysis of joint pressure and velocity measurements, to appear in *Phys. Fluids* (1999).
6. B. Dernoncourt, J.-F. Pinton and S. Fauve: Experimental study of vorticity filaments in a turbulent swirling flow, Physica D (1998).
7. S. Manneville, A. Maurel, F. Bottausci, and Ph. Petitjeans: The "double rotating suction system": Acoustic characterization of a vortex in infinite medium, in this Volume. See also S. Manneville, A. Maurel, C. Prada, M. Tanter and M. Fink: Ultrasound Propagation Through a Rotational Flow: Numerical Methods Compared to Experiments, in proceeding of the 9th International Conference on Theoretical and Computational Acoustics, submitted to The Journal of Computational Acoustics (1999).
8. S. Manneville, J. H. Robres, A. Maurel, P. Petitjeans, and M. Fink: Vortex dynamics investigation using an acoustic technique, Physics of Fluids **11** (11), 3380-3389 (1999).
9. A. La Porta, G.A. Voth, F. Moisy and E. Bodenschatz: Using cavitation to measure statistics of low-pressure events in large-Reynolds-number turbulence, submitted to *Phys. Fluid* (1999).
10. F. Moisy, A. La Porta, G.A. Voth and E. Bodenschatz: Using cavitation as a local pressure probe in turbulence, in this Volume.
11. C. Nore, B. Andreotti, S. Douady and M. Abid: On Burgers' vortex: the missing mechanism, in this Volume.
12. F. Belin, J. Maurer, P. Tabeling and H. Willaime: Observation of intense filaments in fully developed turbulence, *J. Phys II* **6**, 573–584 (1996).